PNAS RESEARCH ARTICLE | MEDICAL SCIENCES OPEN ACCESS

Inhibition of GPR39 restores defects in endothelial cell–mediated neovascularization under the duress of chronic hyperglycemia: Evidence for regulatory roles of the sonic hedgehog signaling axis

Sai Pranathi Meda Venkata[a], Hainan Li[a], Liping Xu[a], Jia Yi Koh[a], Huong Nguyen[a], Morgan Minjares[a], Chunying Li[b], Anjaneyulu Kowluru[a,c], Graeme Milligan[d], and Jie-Mei Wang[a,e,1]

Edited by Napoleone Ferrara, University of California San Diego, La Jolla, CA; received May 19, 2022; accepted November 21, 2022

Impaired endothelial cell (EC)–mediated angiogenesis contributes to critical limb ischemia in diabetic patients. The sonic hedgehog (SHH) pathway participates in angiogenesis but is repressed in hyperglycemia by obscure mechanisms. We investigated the orphan G protein–coupled receptor GPR39 on SHH pathway activation in ECs and ischemia-induced angiogenesis in animals with chronic hyperglycemia. Human aortic ECs from healthy and type 2 diabetic (T2D) donors were cultured in vitro. GPR39 mRNA expression was significantly elevated in T2D. The EC proliferation, migration, and tube formation were attenuated by adenovirus-mediated GPR39 overexpression (Ad-GPR39) or GPR39 agonist TC-G-1008 in vitro. The production of proangiogenic factors was reduced by Ad-GPR39. Conversely, human ECs transfected with GPR39 siRNA or the mouse aortic ECs isolated from GPR39 global knockout ($GPR39^{KO}$) mice displayed enhanced migration and proliferation compared with their respective controls. GPR39 suppressed the basal and ligand-dependent activation of the SHH effector GLI1, leading to attenuated EC migration. Coimmunoprecipitation revealed that the GPR39 direct binding of the suppressor of fused (SUFU), the SHH pathway endogenous inhibitor, may achieve this. Furthermore, in ECs with GPR39 knockdown, the robust GLI1 activation and EC migration were abolished by SUFU overexpression. In a chronic diabetic model of diet-induced obesity (DIO) and low-dose streptozotocin (STZ)-induced hyperglycemia, the $GPR39^{KO}$ mice demonstrated a faster pace of revascularization from hind limb ischemia and lower incidence of tissue necrosis than GPR39 wild-type ($GPR39^{WT}$) counterparts. These findings have provided a conceptual framework for developing therapeutic tools that ablate or inhibit GPR39 for ischemic tissue repair under metabolic stress.

G protein–coupled receptor 39 | endothelial function | limb ischemia | angiogenesis | hyperglycemia

Significance

GPR39 is an orphan GPR whose physiological ligand and intracellular pathways in ECs remain poorly characterized. Our data indicate that inhibition of GPR39 protects EC functions by enhancing SHH signaling in aortic ECs. Understanding the potential cross-talk between GPR39 activation and SHH signaling in hyperglycemia may form the basis for developing therapeutic approaches to target cardiovascular complications in diabetic patients. Our studies also revealed that genetic ablation of GPR39 significantly improves revascularization after ischemia in vivo in a type 2 diabetic mouse model. Our studies open an avenue to preserving endothelial function and vascular health by targeting GPR39. The development of pharmacological or genetic agents to block GPR39 in ECs may be a fruitful area of future research.

Impaired angiogenesis is a crucial feature in diabetes and a primary contributor to the pathogenesis and progression of peripheral artery disease (PAD). The risk of PAD significantly increases in diabetic patients. It can cause severe foot ulcers and critical limb ischemia (CLI), leading to limb amputation (1–2). The treatment for severe PAD and CLI relies on revascularization surgeries (1). Unfortunately, many patients are unsuitable for such intervention and are left with limited treatment options (3). Hence, new approaches to restoring tissue vascularization are urgently needed. Endothelial cells (ECs) play an essential role in vascular homeostasis and angiogenesis by repairing the injured endothelium, forming new vasculature, and secreting vasoactive factors (4). When the endothelium is exposed to hyperglycemia, an array of intracellular events can trigger endothelial deterioration. This dysfunction represents a crucial feature and pathogenic mechanism of aberrant angiogenesis in patients with PAD (5, 6). Therefore, restoring endothelial function might be an effective strategy to maintain angiogenesis and prevent tissue injury in diabetic patients with PAD.

G protein–coupled receptors (GPCRs or GPRs) are seven-transmembrane domain proteins representing the most prominent family of targets for small-molecule therapies (7, 8). Following stimulation of GPRs by specific agonists, signals are transduced into cells via the activation of heterotrimeric G proteins and/or by recruiting arrestin adapter proteins. Although many GPRs are known and are well characterized, there remain a substantial number of GPRs where cognate ligands or downstream intracellular signaling pathways remain elusive. These GPRs are referred to as "orphan" receptors. Initially identified in 1997 as a potential GPR related to the ghrelin receptor (9), GPR39 remains an orphan with limited small-molecule pharmacology, which has restricted the efforts to understand the range of roles it may play. GPR39 is known to

Author contributions: J.-M.W. designed research; S.P.M.V., H.L., L.X., J.Y.K., H.N., and J.-M.W. performed research; C.L. and A.K. contributed new reagents/analytic tools; S.P.M.V., H.L., L.X., J.Y.K., M.M., C.L., A.K., G.M., and J.-M.W. analyzed data; and S.P.M.V., H.L., G.M., and J.-M.W. wrote the paper.

The authors declare no competing interest.

This article is a PNAS Direct Submission.

[1]To whom correspondence may be addressed. Email: jiemei.wang@wayne.edu.

This article contains supporting information online at https://www.pnas.org/lookup/suppl/doi:10.1073/pnas.2208541120/-/DCSupplemental.

Published December 27, 2022.

be activated by physiological concentrations of Zn^{2+} and mediate many zinc-dependent activities (10–12). However, increasing evidence has suggested that GPR39 also displays ligand-independent constitutive activities. In population studies, associations have been found between polymorphic variants of GPR39 and the onset of pathologies, including cancer, cardiovascular diseases, nutrition, and energy homeostasis (13–16). In animal studies, GPR39 has been reported to participate in adipocyte metabolism (17) and regulate pancreatic islet function (18). In the vascular system, GPR39 is differentially expressed among cell types (19) and modulates critical parameters such as smooth muscle osteogenesis (20), endothelial homeostasis (21), and vascular macrophage inflammation (22). While there is insufficient evidence to unequivocally link GPR39 and its mechanism of action to clinical manifestations, its association with cardiometabolic disorders, in combination with its engagement in various cellular and molecular mechanisms contributing to PAD, warrants the study of its role in regulating EC function and in vivo neovascularization in the diabetic environment.

The sonic hedgehog (SHH) pathway robustly regulates embryonic development and angiogenesis and is integral for intercellular communication in ECs (23–25). In the absence of the ligand SHH, the 7-transmembrane domain protein receptor smoothened (SMO) is inhibited by the 12-transmembrane domain protein Patched-1 (PTCH1) (26). The canonical signaling occurs when SHH binds and inactivates PTCH1, releasing SMO to initiate downstream signaling cascades. The translocation of the transcriptional factor glioma-associated oncogene homologue (GLI, GLI1 is the dominant isoform) to the nucleus subsequently activates target gene expressions (27, 28). Alternatively, GLI1 activation can be suppressed by the cytosolic protein suppressor of fused (SUFU). SUFU directly binds GLIs to inhibit the translocation of GLIs to the nucleus, preventing GLI from basal or ligand-dependent activation (29). To date, the upstream regulation of SUFU is not entirely understood. A previous study discovered GPR39 as a potential receptor to mediate the action of synthetic HH signaling inhibitors in a SMO-independent manner (13). However, the putative roles of these signaling pathways in the context of EC functions remain unexplored. Extant studies, including ours, have demonstrated that SHH pathway activation can boost neovascularization in ischemic tissue but is defective in hyperglycemia (30, 31). Investigations into the mechanisms controlling this pathway will advance our understanding of impaired neovascularization and potentiate therapeutic interventions. Whether GPR39 modulates SHH signaling in ECs remains unknown as the molecular basis for such an effect has not been established. Therefore, we sought to test whether the SHH pathway is an essential target for GPR39 to modulate EC behavior and production of cytokines.

In this study, we examined the impact of GPR39 knockdown and knockout on angiogenesis in human and mouse aortic ECs (MAECs) in vitro. We assessed the effect of modulation of GPR39 levels and activity on the production of EC-derived angiogenic factors. Furthermore, we tested whether the SHH signal plays an essential role in GPR39-regulated angiogenesis. Using a mouse model of obesity and chronic hyperglycemia, we evaluated the therapeutic potential of GPR39 inhibition in the restoration of blood perfusion and tissue repair upon ischemic injury with the premise that understanding the interactions between GPR39 and the SHH pathway in hyperglycemic conditions may identify therapeutic approaches to target cardiovascular complications in diabetic patients.

Results

GPR39 Expression Dictates EC Dysfunction. ECs from diabetic donors demonstrate impaired angiogenic ability in vitro. Consistent with this observation, we noted the reductions of proliferation (Fig. 1*A*), migration (Fig. 1*B*), and 3D tube formation (Fig. 1*C*) of type 2 diabetic (T2D) human ECs compared with healthy human ECs. In T2D ECs, GPR39 mRNA levels were significantly higher than in the healthy controls (Fig. 1*D*). Next, we transfected the healthy ECs with adenovirus carrying human GPR39 gene (Ad-GPR39, 30 MOI, 48 h). Real-time PCRs confirmed the overexpression of GPR39 mRNA levels (*SI Appendix*, Fig. S1*A*). Functional assays suggested that proliferation (Fig. 1*E*), migration (Fig. 1*F*), and tube formation (Fig. 1*G*) were impaired. Moreover, the addition of the small-molecule GPR39 agonist, TC-G-1008, to ECs from either healthy or T2D patients resulted in reduced cell proliferation (Fig. 1 *H* and *I*) and migration (Fig. 1 *J* and *K*). GPR39 is known to display substantial levels of ligand-independent constitutive activity (32, 33). The above results suggest that both constitutive and ligand-stimulated GPR39 activities can regulate EC functions. By contrast, effective knockdown of GPR39 mRNA levels (*SI Appendix*, Fig. S1*B*) significantly enhanced proliferation (Fig. 1*L*), migration (Fig. 1*M*), and tube formation (Fig. 1*N*) of ECs from healthy subjects and migration of ECs from T2D donors (Fig. 1*O*). Similarly, ECs isolated from GPR39 global knockout ($GPR39^{KO}$) mice displayed enhanced migration (Fig. 1*P*) and tube formation (Fig. 1*Q*) compared with their wild-type counterparts ($GPR39^{WT}$). There was also a trend toward the enhanced proliferation of $GPR39^{KO}$ mouse ECs, but this was not statistically significant (Fig. 1*R*; $P = 0.0931$ vs. $GPR39^{WT}$ ECs). These observations demonstrate an inhibitory role of GPR39 in EC angiogenesis in humans and mice.

Overexpression of GPR39 Suppresses EC-Derived Angiogenic Factors. The ECs participate in neovascularization by forming the vessels and/or secreting vasoactive cytokines/growth factors to facilitate the process. In addition to examining EC behavioral changes, we also assessed the EC-derived cytokine/growth factor profile following GPR39 overexpression using a comparative Proteome Profiler array of 55 different angiogenic mediators. Fig. 2*A* shows the relative abundance of these factors. We found that GPR39 overexpression significantly reduced the protein levels of many critical angiogenic factors, including vascular endothelial growth factor (VEGF), interleukin-8 (IL-8), coagulation factor-III (Cog factor III), epithelial growth factor (EGF), angiopoietin-1 (ANG1), serpin E1, and dipeptidyl peptidase IV (DPP IV), in ECs from healthy subjects (Fig. 2 *B* and *C*). In parallel, real-time PCR analyses showed significant downregulation of mRNA levels of these molecules following GPR39 overexpression (Fig. 2*D*), suggesting that suppression of the angiogenic factors by GPR39 is mediated at the transcriptional level. Only two molecules, placental growth factor (PIGF) and platelet-derived growth factor AB (PDGF-AB), were decreased at mRNA levels but increased at protein levels upon GPR39 overexpression (Fig. 2 *C* and *D*). In line with the protein array, the culture media collected from ECs overexpressing GPR39 (treated with Ad-GPR39 using Ad-GFP as controls) inhibited EC migration in vitro (Fig. 2*E*), while the addition of such medium to ECs with GPR39 knockdown (transfected with GPR39 siRNA using scrambled oligonucleotides as controls) stimulated EC migration (Fig. 2*F*). Furthermore, we tested the requisite nature of these proangiogenic factors, including serpin E1, EGF, VEGF, IL-8, Cog factor III, and ANG1, in GPR39-modulated EC angiogenesis by simultaneously knocking down GPR39 and each of these angiogenic factors,

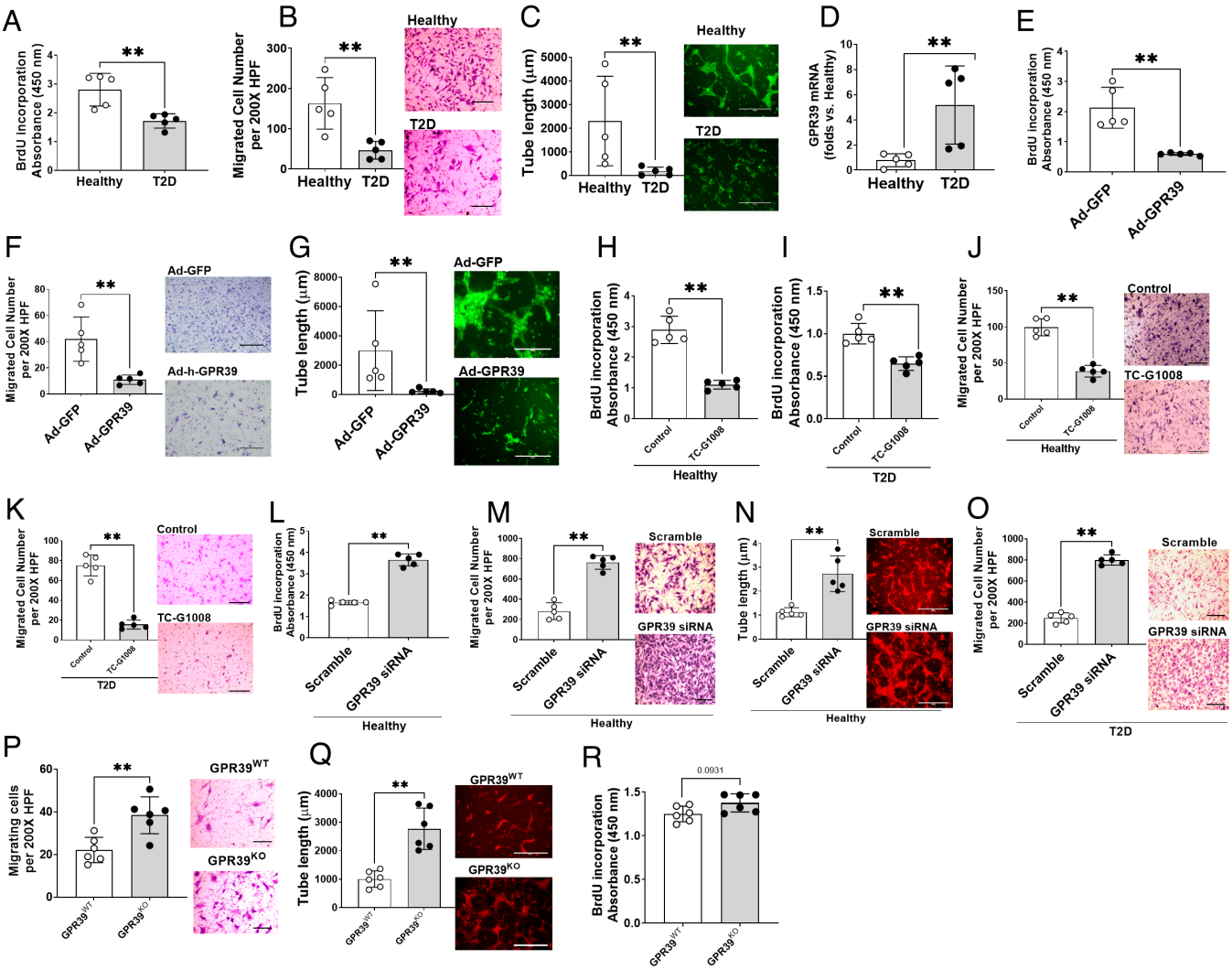

Fig. 1. Overexpression of GPR39 results in deterioration of EC function and GPR39 suppression rescues (EC functions). The functions of human aortic ECs from healthy and T2D donors were evaluated by proliferation (*A*), migration (*B*), and 3D tube formation (*C*). In each assay, n = 5 per group, $^{**}P < 0.01$. (*D*) The up-regulated GPR39 mRNA levels in T2D ECs compared with healthy ECs. n = 5 per group, $^{**}P < 0.01$. Healthy ECs transfected with adenovirus carrying human GPR39 gene with a GFP tag (Ad-GPR39) demonstrated impaired proliferation (*E*), migration (*F*), and 3D tube formation (*G*) compared with adenovirus carrying *egfp* (Ad-GFP)-treated controls. n = 5 per group. GPR39 agonist TC-G-1008 impaired proliferation (*H* and *I*) and migration (*J* and *K*) in healthy and T2D ECs. n = 5, $^{**}P <$ 0.01 vs. per group. Functional assays determined that healthy ECs transfected with siRNA targeting human GPR39 (GPR39 siRNA) had enhanced proliferation (*L*), migration (*M*), and 3D tube formation assay (*N*) compared with the control group transfected with a scrambled siRNA (scramble). n = 5 per group, $^{**}P < 0.01$. In T2D ECs, GPR39 siRNA significantly augmented migration (*O*). n = 5 per group, $^{**}P < 0.01$. Similarly, $GPR39^{KO}$ MAECs show enhanced migration (*P*) and 3D tube formation (*Q*) compared with $GPR39^{WT}$ MAECs. n = 6 per group, $^{**}P < 0.01$. The cell proliferation indicated a trend toward enhanced proliferation in $GPR39^{KO}$ MAECs but did not reach significance (*R*). All the figures show representative images next to the dot plot figure. (Scale bars, 200 μm in migration and 400 μm in 3D tube formation.) HPF, high-power field. Data are presented as mean ± SD. *P* values were determined by the Mann–Whitney *U* test.

followed by the evaluation of EC function using the migration assay. Our data suggested that serpin E1, Cog factor III, IL-8, and ANG1 were essential for GPR39-modulated EC migration (Fig. 2 *G* and *F*). IL-8 and serpin E1 were most significant. Although VEGF appeared to also contribute, this was not statistically significant. Notably, knocking down each of these factors did not completely blunt the increased EC migration by GPR39 knockdown, suggesting that multiple factors are contributing to GPR39-modulated angiogenesis.

Deletion of GPR39 Augments the SHH Signaling Pathway. Next, we sought to understand the mechanism(s) transducing suppression of various angiogenic genes by GPR39. The SHH pathway is a potent angiogenic pathway through its effector GLI. We determined whether the SHH module is essential for GPR39-mediated EC function. Indeed, the enhanced EC migration in response to GPR39 knockdown was blunted by the simultaneous knockdown of GLI (Fig. 3*A*). Similarly, silencing GLI1 in $GPR39^{KO}$ ECs significantly limited cell migration (Fig. 3*B*), suggesting an essential role of the SHH pathway in GPR39-modulated EC function. Next, we used a GLI-luciferase reporter assay to determine the activation of the SHH pathway in ECs in which the expression of GPR39 was manipulated. The luciferase signal indicates GLI1 activation in the nucleus. GLI1 activity was increased following GPR39 knockdown in ECs from both healthy (Fig. 3*C*) and T2D subjects (Fig. 3*D*) in both basal conditions and upon the addition of SHH ligand. Although not achieving statistical significance, a similar trend was noted in ECs from both $GPR39^{KO}$ and $GPR39^{WT}$ mice (Fig. 3*E*). In contrast, adenovirus-mediated gene transfer of GPR39 limited both constitutive and ligand-dependent GLI1 activations (Fig. 3*F*). These results suggest that the loss of GPR39 is sufficient to activate GLI1 without ligand

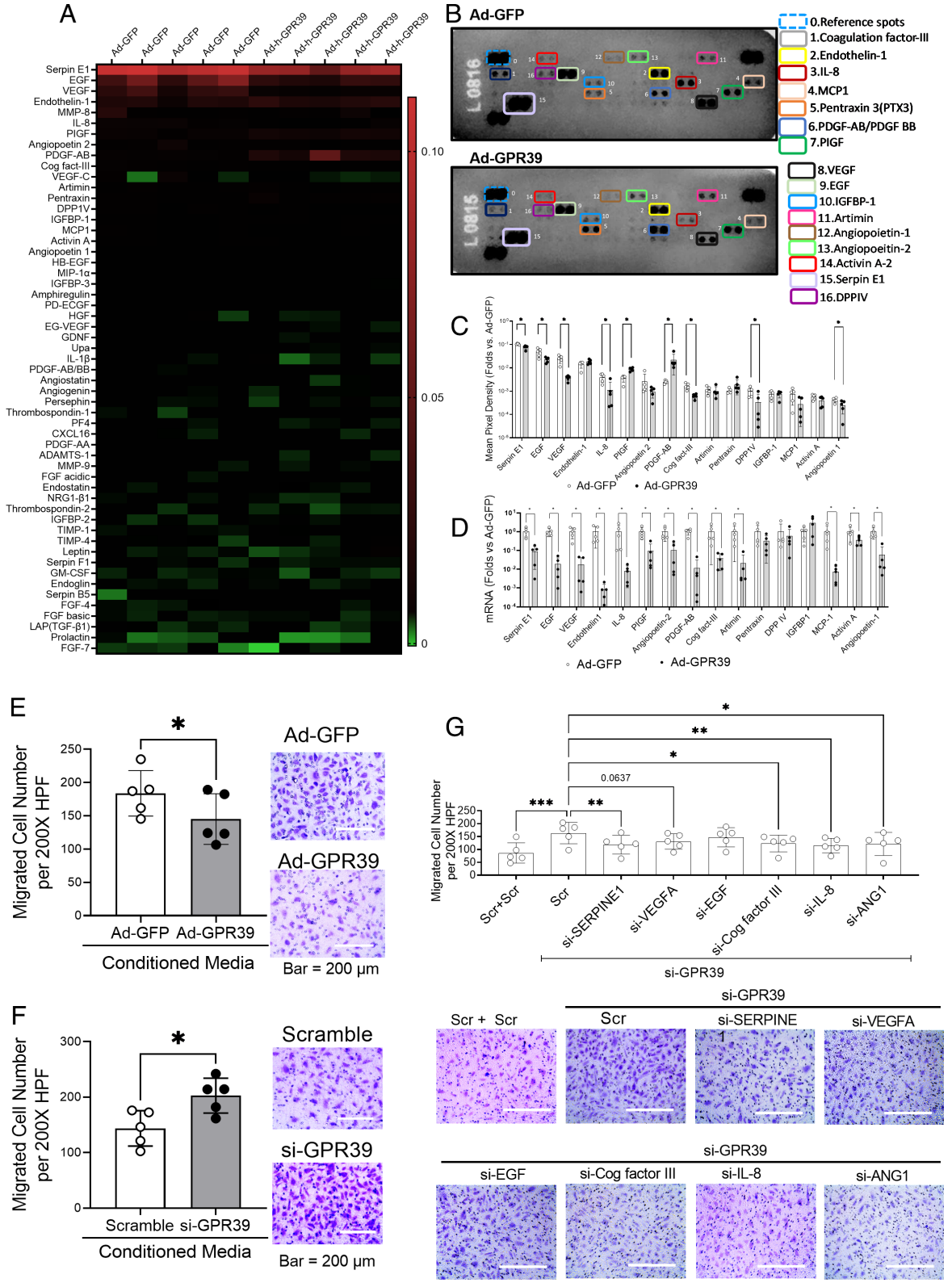

Fig. 2. GPR39 suppresses EC-derived angiogenic factors. (*A*) Heat map generated from the Proteome Profiler Human Angiogenesis Array reflecting protein expression values of 55 proteins in human aortic ECs transfected with adenovirus carrying GFP (Ad-GFP) or adenovirus carrying human GPR39 (Ad-GPR39). Samples are arranged in columns (n = 5 per group), and proteins are arranged in rows. Red shades show increased expression of angiogenesis array proteins; green shades indicate reduced expression, and black indicates median expression. (*B*) Representative images of the Proteome Profiler Human Angiogenesis Array from the same sample transfected with Ad-GFP (*Top*) and Ad-GPR39 (*Bottom*). n = 5 per group. The angiogenic mediators with statistical significance are shown using colored rectangles. The unlabeled spots represent other angiogenic mediators that did not show a statistical difference between the control and treatment groups. (*C*) Quantification of densitometric values of angiogenesis mediators from the Proteome Profiler Human Angiogenesis Array. n = 5 per group, $^*P < 0.05$. (*D*) mRNAs corresponding to the protein array angiogenesis mediators. n = 5 per group, $^*P < 0.05$. (*E*) Healthy ECs were transfected with Ad-GPR39 or Ad-GFP for 48 h. Conditioned media were collected to use on ECs for the migration assay. n = 5 per group, $^*P < 0.05$. (*F*) Healthy ECs were transfected with GPR39 siRNA or scrambled oligos for 48 h. Conditioned media were collected to use on ECs for the migration assay. n = 5 per group, $^*P < 0.05$. (*G*) Migration assay of healthy ECs transfected with GPR39 siRNA together with scramble control, siRNA against human serpine E1 (si-SERPINE1), vascular endothelial growth

binding to canonical membrane receptors. The observation further supported that cyclopamine, a known inhibitor of SMO, could not abolish the ligand-dependent activation when GPR39 was knocked down by siRNA (Fig. 3*G*). Together, these observations suggest that GPR39 interferes with the SHH pathway at the postmembrane receptor level, suggesting that the interaction molecule(s) is downstream of SMO in the SHH pathway. We then measured the protein levels of molecules within the SHH signaling pathway in GPR39-manipulated ECs. PTCH1 and GLI1 protein levels were elevated in ECs from GPR39^{KO} mice (Fig. 3*H*), which supported the activation of SHH pathway because GLI1 and PTCH1 are conserved SHH pathway targets, and their expressions are typically used to measure SHH signaling activity (34). On the other hand, PTCH1 and GLI1 protein levels decreased upon Ad-GPR39 transfection, while SHH, SMO, and SUFU remained comparable (Fig. 3*I*). To determine the molecular basis for GPR39 regulation of SHH signaling, we conducted coimmunoprecipitation (Co-IP) experiments. GFP-tagged GPR39 was pulled down for the detection of its binding partners. Our data indicated that GPR39 directly interacted with SUFU but not with SHH, PTCH1, SMO, or GLI1 (Fig. 3*J*). These findings suggest that, through binding with SUFU, the negative regulator downstream of SMO, GPR39 inhibition relieves the suppression of SUFU on GLI1 activation, bypassing the canonical membrane receptors and initiating the downstream signaling pathway cascade. Indeed, the GLI-luciferase reporter assay suggested that reinstallation of SUFU (by an expression plasmid carrying human SUFU) led to complete suppression of GLI1 activation permitted by GPR39 siRNA at the basal level upon SHH ligand stimulation (Fig. 3*K*). The robust migration induced by GPR39 knockdown was completely abolished by the restoration of SUFU (Fig. 3*L*). Furthermore, to test whether increased glucose level stimulates GPR39 signaling and GPR binding to SUFU, we exposed ECs to high glucose (25 mM for 72 h). Our data indicated that there was a trend of increased GPR39 mRNA expression under high-glucose conditions, but this was not statistically significant ($P = 0.0625$; Fig. 3*M*). GLI1 activation was attenuated under high-glucose conditions and was further worsened by the overexpression of GPR39 (Fig. 3*N*). This is possibly related to the enhanced binding of GPR39 to SUFU, as indicated by the coimmunoprecipitation assay (Fig. 3*O*).

GPR39 Deletion Accelerates Ischemia-Induced Neovascularization in Hyperglycemia In Vivo. Tissue ischemia is one of the strongest stimuli of neovascularization in vivo in which ECs play a vital role (35). The hind limb ischemia model and PAD patients with CLI frequently show similar neovascularization patterns with arteriogenic responses of remodeling collateral arteries in proximal tissue and angiogenic response of forming capillaries in distal ischemic tissue (35, 36). When hind limb ischemia surgery is performed in animals with chronic pathologies, such as hyperglycemia and atherosclerosis, this model is the most used to mimic the clinical situation of PAD patients where comorbidities are present (37–39). We created an obese and a chronic hyperglycemia model in GPR39^{WT} and GPR39^{KO} mice using the schema highlighted in Fig. 4*A*, based on previously published protocols (40). Diet-induced obesity (DIO) was induced over 10 wk before animals were rendered hyperglycemic by five injections of low-dose streptozotocin (STZ) for an additional 8 wk (~2 mo), while the high-fat diet was continued. Such a protocol models pathologies in human type 2 diabetes, including obesity, insulin resistance, and hyperglycemia. A standard diet with STZ injections served as a hyperglycemic group, and DIO with citrate buffer injections served as a nondiabetic obese control. In male GPR39^{WT} mice, the high-fat diet induced weight gain and blood glucose increase, but blood glucose levels stayed unchanged in females (*SI Appendix*, Fig. S2 *A* and *B*). At each checkpoint (DIO at 16 wk and DIO + STZ at 24 wk), there was a significant difference in body weight and blood glucose between males and females. We monitored the blood glucose levels of both females and males receiving STZ for 12 wk. Our results showed that both male GPR39^{KO} and GPR39^{WT} mice developed moderate hyperglycemia, but female GPR39^{KO} and GPR39^{WT} mice remained normoglycemic until 12 wk (*SI Appendix*, Fig. S2*C*). This sex-specific dimorphism was consistent with previous reports that male but not female mice are prone to DIO and STZ-induced hyperglycemia (41–43), and estrogen has been speculated to play a protective role in metabolic homeostasis against nutrient or pharmacological stress (44). We performed femoral arterial ligation in these animals. There are variations in surgical procedures of inducing hind limb ischemia that impact on neovascularization assessment (36). We used the double ligations of the femoral arteries (one was distal to the origin of the deep branch, and the other was above the bifurcation of the saphenous and popliteal arteries), which created a higher degree of tissue ischemia and damage, allowing us to evaluate both arteriogenesis (the remodeling of the collateral arteries) in the thigh muscles and angiogenesis (capillary formation) in the calf muscle. The blood flow recovery was monitored by a laser Doppler imager, while tissue necrosis was assessed and scored for 4 wk after surgery. In the STZ-induced chronic hyperglycemia model, GPR39^{KO} mice restored blood perfusion faster than GPR39^{WT} mice (Fig. 4 *B* and *C*), while there was no difference between GPR39^{KO} and GPR39^{WT} mice when they were normoglycemic (Fig. 4*B*). The GPR39^{KO}-STZ (hyperglycemic but not obese) mice had developed increased arteriolar numbers compared with GPR39^{WT}-STZ (Fig. 4 *D* and *E*), with a tendency to form larger arteries ($P = 0.0753$; Fig 4*F*), as measured by immunofluorescent staining of α-smooth muscle actin (SMA) and CD31 (also known as platelet EC adhesion molecule, PECAM-1). The capillary density in the calf muscle was higher in GPR39^{KO}-STZ than that in GPR39^{WT}-STZ mice (Fig. 4*G*), as measured by immunohistological staining for CD31. The recovery curve of blood perfusion was comparable between DIO-GPR39^{KO} mice and DIO-GPR39^{WT} mice (Fig. 4 *H* and *I*). Indeed, no differences were found between SD-GPR39^{KO}, GPR39^{WT}-SD, GPR39^{KO}-DIO, and GPR39^{WT}-DIO mice. However, in the DIO + STZ model, the GPR39^{KO} mice displayed a significant acceleration of blood perfusion recovery compared with GPR39^{WT} mice (Fig. 4 *H* and *I*). The muscles from GPR39^{KO}-DIO + STZ (hyperglycemic and obese, considered mimicking type 2 diabetes) mice showed higher arterial numbers (Fig. 4 *J* and *K*) and more

factor (si-VEGFA), epithelial growth factor (si-EGF), interleukin-8 (si-IL-8), coagulation factor-III (si-Cog factor III), and angiopoietin 1 (si-ANG1) for 48 h using double amount of scrambled oligo as control. The quantification is shown in *Top* panel, and representative images of migrated cells were shown in *Lower* panel. Data are represented as mean ± SD. When a comparison was made between two groups, *P* values were determined by the Mann–Whitney *U* test. The *P* values were determined by the Mann–Whitney *U* test. When a comparison was made between more than two groups of treatments, the *P* values were first determined by the Kruskal–Wallis test across all the groups, and if significant, the pairs of primary interest, based on scientific rationale, were assessed using the Mann–Whitney *U* test with Benjamini, Krieger, and Yekutieli's adjustment for multiple comparisons. The significant differences that came from post hoc comparisons of groups were noted.

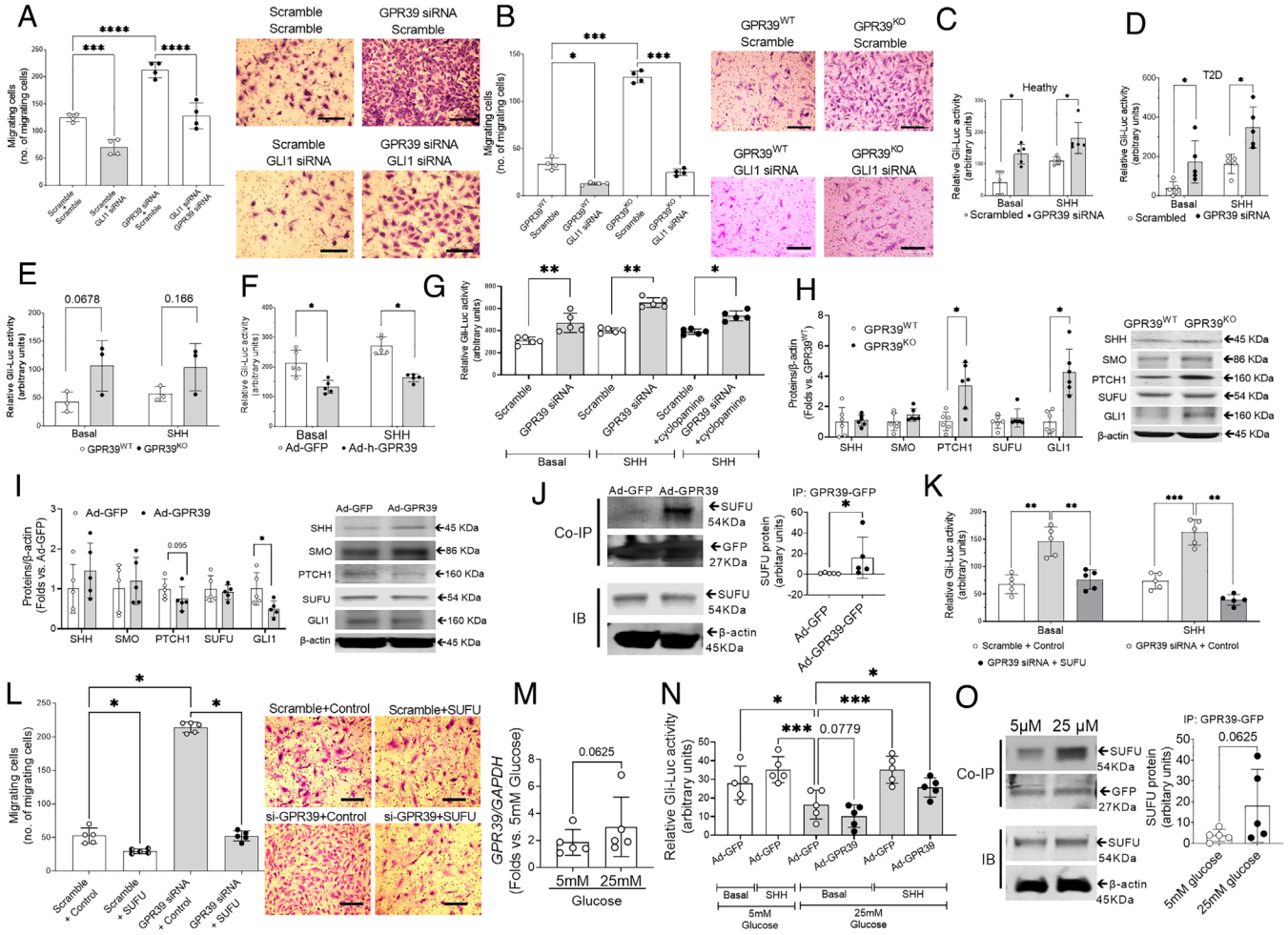

Fig. 3. GPR39 suppresses the activation of the SHH pathway. (*A*) The migration of human ECs transfected with GLI1 siRNA and/or GPR39 siRNA using transfection of scramble sequence as control. n = 4 per group; ***P < 0.001 and ****P < 0.0001. (Scale bar, 200 μm.) (*B*) The migration of GPR39^{KO} and GPR39^{WT} MAECs receiving GLI1 siRNA or scramble controls. n = 4 per group; *P < 0.05 and ***P <0.001. (Scale bar, 200 μm.) GLI-luciferase reporter assays revealed that silencing GPR39 increased the GLI1 activation at the basal levels and upon SHH peptide stimulation in healthy ECs (*C*) and T2D ECs (*D*). n = 5 per group, *P < 0.05. GPR39^{KO} MAECs showed a trend of increased GLI1 activation compared with GPR39^{WT} ECs (*E*). On the contrary, overexpression of GPR39 by adenovirus-mediated human GPR39 gene transfer (Ad-GPR39) significantly reduced GLI1 activation (*F*). n = 5 per group; *P < 0.05 and **P < 0.01. (*G*) GLI1 activation at the basal level and upon SHH peptide stimulation in healthy human ECs transfected by GPR39 siRNA with or without simultaneous treatment of SMO inhibitor cyclopamine (5 μM) using transfection of scramble sequence as control. The GLI1 activation was measured by the GLI1-luciferase reporter assay. n = 5 per group, *P < 0.05. (*H*) Protein expression of SHH, SMO, Patched-1 (PTCH1), SUFU, and GLI1 in GPR39^{WT} and GPR39^{KO} MAECs. n = 5 per group, *P < 0.05. (*I*) Protein expression of SHH, SMO, PTCH1, SUFU, and GLI1 in healthy human ECs transfected with Ad-GPR39 or Ad-GFP. n = 5 per group. (*J*) Coimmunoprecipitation (Co-IP) of GPR39 and SHH pathway proteins. Healthy human ECs were transfected with Ad-GPR39-GFP or Ad-GFP. The GPR39 was pulled down by an antibody against its GFP tag. The Co-IP protein lysate was probed for SHH pathway proteins, including SHH, PTCH1, SMO, SUFU, and GLI1. Of these, only SUFU showed binding with GPR39-GFP but not SHH, PTCH1, SMO, or GLI1. The quantification of coimmunoprecipitated SUFU was shown in the *Left* panel. The representative bands of SUFU in Co-IP protein lysate and SUFU in immunoblotting (IB) of whole-cell lysate from the same sample were shown in the *Right* panel. n = 5 per group, *P < 0.05. (*K*) GLI1 activation at the basal level and upon SHH peptide stimulation in healthy human ECs transfected by GPR39 siRNA with or without simultaneous transfection of SUFU overexpression plasmid (48 h) using transfection of scramble sequence and control plasmid as control. The GLI1 activation was measured by the GLI1-luciferase reporter assay. n = 5 per group. **P < 0.01; ***P < 0.001. (*L*) The migration of human ECs transfected with GPR39 siRNA with or without simultaneous transfection of SUFU overexpression plasmid (40 ng/10^4 cells, 48 h) using transfection of scramble sequence and control plasmid as control. n = 4 per group, *P < 0.05. (Scale bar, 200 μm.) (*M*) GPR39 mRNA levels in healthy ECs exposed to high-glucose condition (25 mM) for 72 h using 5 mM glucose and 20 mM mannitol as control. n = 5. (*N*) GLI1 activation at the basal level and upon SHH peptide stimulation in human ECs exposed to high-glucose condition (25 mM) for 72 h at the basal level and upon SHH peptide stimulation using 5 mM glucose and 20 mM mannitol as control. The GLI1 activation was measured by the GLI-luciferase reporter assay. n = 5. *P < 0.05; ***P < 0.001. (*O*) Co-IP of GPR39 and SUFU protein. Healthy human ECs were transfected with Ad-GPR39 or Ad-GFP followed by 72 h of 25 mM or 5 mM glucose treatment. The GPR39 was pulled down by an antibody against its GFP tag. The coimmunoprecipitated protein lysate was probed for SUFU protein. The quantification of coimmunoprecipitated SUFU in Co-IP protein lysate is shown. In all the figures, data are represented as mean ± SD. When a comparison was made between two groups, the P values were determined by the Mann–Whitney U test. When a comparison was made between more than two groups of treatments, the P values were first determined by the Kruskal–Wallis test across all the groups, and if significant, the pairs of primary interest, based on scientific rationale, were assessed using the Mann–Whitney U test with Benjamini, Krieger, and Yekutieli's adjustment for multiple comparisons. The significant differences that came from post hoc comparisons of groups were noted.

prominent arteries (Fig. 4*L*) compared with those from GPR39^{WT} counterparts. The robust arteriogenesis in GPR39^{KO}-DIO+STZ mice was accompanied by augmentation of capillary density in the calf muscle (Fig. 4*M*). Furthermore, the incidence of necrotic tissue was lower in GPR39^{KO} than in GPR39^{WT} mice in both the DIO and DIO-STZ models (Fig. 4*N*). No necrosis was observed in DIO-GPR39^{KO} mice, and only one DIO + STZ GPR39^{KO} mouse developed tissue necrosis. These observations further substantiate our hypothesis that GPR39 deletion protects tissue recovery from ischemia-induced injury, and this was attributed to enhanced arteriogenesis and angiogenesis.

In the female mouse study, we continued to monitor body weight and blood glucose in females receiving a high-fat diet for an extended period. Both GPR39^{KO} and GPR39^{WT} female mice showed a mild

body weight gain but did not display hyperglycemia until 26 wk of maintenance on the high-fat diet (Fig. 4 *O* and *P*). In the DIO + STZ group, the female mice displayed obesity and hyperglycemia at the 27th wk (33 wk of age). Although there was no difference in blood glucose values between female GPR39^{KO} and GPR39^{WT} mice, the body weights of female GPR39^{WT}DIO-STZ mice tended to be higher than those of female GPR39^{KO} DIO-STZ mice at 40 wk (Fig. 4*O*). Once they became obese and hyperglycemic (~13 wk after STZ injections), hind limb ischemia surgery was performed, and the blood perfusion recovery was recorded. Our data showed that GPR39^{KO} females performed much better in recovering blood perfusion (Fig. 4*Q*) and preserving tissue viability in ischemia than GPR39^{WT} females (Fig. 4*R*), consistent with our findings in the males.

Discussion

In this study, we have identified a role for GPR39 in EC-mediated neovascularization: an antiangiogenic signaling molecule independent of its function as a zinc sensor. Support for this role has come from its elevated expression in ECs from T2D patients, its inhibition of EC functions in vitro, its attenuation of the SHH pathway at the levels of both constitutive and ligand-stimulated activation, and its critical function in revascularization during tissue ischemia in T2D animals in vivo. Genetic or pharmacological inhibition of GPR39 benefits EC functions in vitro, restoring SHH pathway activation, revitalizing neovascularization, and protecting against tissue necrosis under chronic metabolic stress in vivo (Fig. 5). GPR39 binds with SUFU and enhances its inhibition of GLI1. In diabetes, the elevated GPR39 initiated the downstream signaling cascades by enhancing the inhibition of SUFU on GLI1 activation, suppressing EC function and endothelium-derived cytokines and growth factors for neovascularization. Together, these data strongly suggest regulatory roles for GPR39 based on its robust interactions with the SHH pathway, potentially affecting therapeutic angiogenesis.

We observed several differences from previously reported outcomes concerning the in vivo studies despite these clear outcomes. For example, altered metabolism in adipocytes from GPR39^{KO} mice has previously been reported in response to a high-fat diet (45), and mpaired glucose-stimulated insulin secretion was found both in vivo and in vitro (18). However, another study failed to distinguish differences in body weight, food intake, glucose, and insulin levels between GPR39^{KO} and GPR39^{WT} mice at young ages (46). In our pilot studies, GPR39^{KO} mice at 24 wk of age possessed lower fasting blood glucose compared with GPR39^{WT} mice (*SI Appendix*, Fig. S3*A*), with intact glucose tolerance (*SI Appendix*, Fig. S3*B*) and insulin response (*SI Appendix*, Fig. S3*C*). In the DIO-STZ model, there were no significant differences in body weight (*SI Appendix*, Fig. S4*A*) or blood glucose levels (*SI Appendix*, Fig. S4*B*) between GPR39^{KO} and GPR39^{WT} mice. It may be germane to point out that age seems to be a significant factor affecting the physiological roles of GPR39 because most of the positive findings on glucose metabolism or insulin sensitivity induced by GPR39 deletion were observed in aged animals. Given that a large proportion of T2D patients is from the more aging population, future investigations into GPR39-induced age-related mechanisms in glucose metabolism appear to be a fertile area for investigation. Nonetheless, our in vivo studies in male and female GPR39^{KO} mice have clearly demonstrated an enhanced protective phenotype against ischemia injury and acceleration of tissue repair induced by GPR39 deletion (Fig. 4), suggesting the potential efficacy of GPR39-based therapeutic intervention in patients with PAD.

The EC-derived cytokines and growth factors are pivotal to neovascularization in response to ischemic tissue injury. Our data showed that GPR39 suppressed multiple proangiogenic factors produced by ECs, particularly those with high abundance and high proangiogenic potency, for example, serpin E1, VEGF, EGF, IL-8, and ANG1 (Fig. 2*C*). Meanwhile, GPR39 also regulates EC-derived proarteriogenic factors, such as MCP1, GM-CSF, and FGF2 (*SI Appendix*, Fig. S5). This observation was consistent with GLI1 activities controlled by GPR39 (Fig. 3*G*) because many of these molecules are target genes of GLI transcription response to SHH signaling (47, 48). We actually tested whether these cytokines/growth factors were due to SHH/GLI1-mediated transcriptional activation by knocking down GLI1 followed by the EC migration assay. Our data indicated that among all GPR39-modulated angiogenic factors, Cog factor III and IL-8 were regulated through GLI1 activation (*SI Appendix*, Fig. S6). Two molecules, PIGF and PDGF, were found to increase protein levels upon GPR39 overexpression despite their decreased mRNA levels. The potential posttranslational regulations that lead to discrepancies in protein and mRNA levels, for example, interactions with translational factors and ribosomes, cellular compartment allocations, or protein stability, remain elusive. In addition, the protein array unveiled the suppressive effect of GPR39 on DPP IV, a multifunctional protein not only promoting angiogenesis but also mediating degradation and inactivation of glucagon-like peptide-1 (GLP-1) (49). Indeed, DPP IV inhibitors are currently in use for the management of type 2 diabetes as they prevent the degradation of GLP-1, thereby maintaining therapeutic levels of GLP-1 in circulation (50). With those differences mentioned above in experimental observations in glucose metabolism in the GPR39^{KO} animals, investigations into tissue- or cell type–specific antagonism of GPR39 are needed to elucidate its therapeutic value.

In the ischemic environment, hypoxia is a key driver for augmenting proangiogenic factor production. We did not observe significant changes in GPR39 mRNA under hypoxia (*SI Appendix*, Fig. S7*A*). The mRNA levels of serpine E1 and VEGFA were significantly increased by hypoxia or ablation of GPR39 (*SI Appendix*, Fig. S7*B*). However, under hypoxia, they were comparable between control and GPR39-depleted cells, suggesting hypoxia did not affect GPR39-modulated proangiogenic factor in ECs. Muscle-derived but not EC-derived proangiogenic molecules would play a key role in neovascularization. To test whether skeletal muscle–derived angiogenic factors took part in the faster recovery of the GPR39^{KO} mice, we recovered the ischemic gastrocnemius muscle samples from GPR39^{KO} and GPR39^{WT} mice on day 7 after the surgery when tissue ischemia was present and robust vascularization response occurred. Any visible vessels or connective tissues were removed from the samples as much as possible to ensure that skeletal muscles remained the predominant content. Our results demonstrated comparable mRNA levels of VEGF, EGF, IL-8, Cog factor III, serpin E1, and ANG1 in ischemic GPR39^{KO} and GPR39^{WT} muscles (*SI Appendix*, Fig. S7*C*), suggesting that similar to ECs, the regulation of GPR39 on angiogenic factor production was not altered in hypoxia.

Apart from these contradictory results of GPR39 regulation of body weight and glucose metabolism, the biological function of GPR39 has been attributed to the sensing and mediating of the physiological functions of Zn^{2+}. Because Zn^{2+} is an essential mineral that regulates various biological molecules (e.g., transcription factors, enzymes, and others), the studies of GPR39 have been focusing on growth, morphogenesis, immune response, neurosensory, and endocrine functions (51). However, manipulating GPR39 does not always reconcile alterations in cellular function based on alterations in Zn^{2+} levels. For

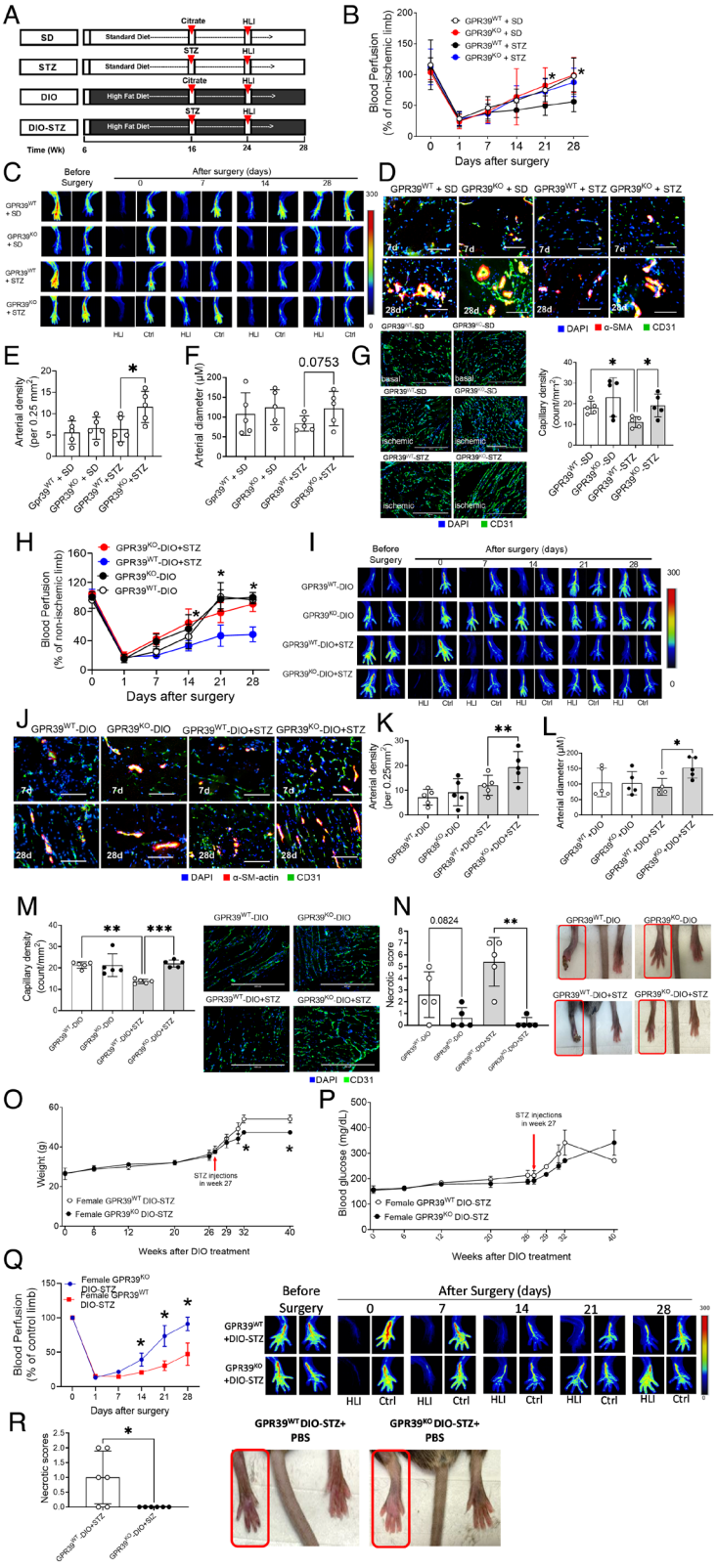

Fig. 4. Genetic deletion of GPR39 facilitates ischemia-induced angiogenesis in male and female mice with chronic hyperglycemia. (*A*) Protocols used to develop animal models of chronic conditions, including hyperglycemia induced by low-dose STZ injections, high-fat (HF) diet–induced obesity (DIO), and type 2 diabetes induced by both DIO plus low-dose STZ injections using standard diet (SD) plus vehicle (citrate buffer) injection as healthy control. Hind limb ischemia was created in these animals by unilateral femoral artery ligation. A laser Doppler imager was used to monitor the blood perfusion during the recovery phase (4 wk). The perfusion index was calculated by the percentage of blood perfusion read in the ischemic limb to that in sham surgery–operated limb in the same animal. (*B*) Blood perfusion in the male GPR39^{WT} and GPR39^{KO} mice with STZ-induced hyperglycemia. n = 5 per group, *P < 0.05 vs. GPR39^{WT}-STZ at the same time point. Representative images of blood perfusion are shown at (*C*). The collateral arteries in the media thigh muscles harvested on day 7 and day 28 after surgery were evaluated by fluorescent staining of anti-α-SMA and CD31. Representative images are shown in (*D*), and the quantification of arterial density and arterial diameter in day 28 samples are shown in (*E*) and (*F*), respectively. n = 5 per group, *P < 0.05. (Scale bar, 200 μm.) (*G*) The capillary density of ischemic muscle sections from GPR39^{WT}-SD, GPR39^{KO}-SDGPR39^{WT}-STZ, and GPR39^{KO}-STZ mice by CD31 fluorescent staining. n = 5 per group, *P < 0.05. Representative images are shown in the *Right* panel. (Scale bar, 400 μm.) (*H*) Blood perfusion in the male GPR39^{WT} and GPR39^{KO} mice with type 2 diabetes induced by DIO + STZ

example, at micromolar levels, Zn^{2+} promotes EC survival in vitro (52). Moreover, the GPR39 agonist TC-G-1008 decreases macrophage inflammatory response and monocyte attachment to ECs when challenged with oxidized low-density lipoprotein in vitro (53). Zinc is an essential element in cell culture, and the sera used at 5 to 10% in the culture media provide sufficient Zn^{2+} (ranging from picomolar to single-digit nanomolar) for cell growth and survival. Our in vitro experiments demonstrated that at low Zn^{2+} levels, GPR39 overexpression or activation by TC-G-1008 in ECs resulted in detrimental consequences, distinct from previous findings at physiological concentrations of Zn^{2+} or in immune cells, suggesting that endothelial GPR39 might mediate activities through an endogenous ligand in an autocrine manner, independent of its function as a Zn^{2+} sensor. It is beyond the scope of the current study to screen for physiologically relevant endogenous ligands apart from Zn^{2+} for endothelial GPR39. However, our in vivo studies in which physiological concentrations of Zn^{2+} were present show that inhibition of GPR39 promotes EC angiogenesis and facilitates tissue recovery from ischemic injury.

Another potential limitation of our study was that we utilized macrovascular ECs because they are more stable than microvascular ECs, which are known to rapidly lose their endothelial characteristics in cell culture with passages and are prone to senescence (54). However, we also appreciate the heterogeneity of ECs at different anatomic locations of the vascular tree (55). To better capitulate EC behaviors in limb ischemia in vivo, skeletal muscle microvascular ECs may be suitable for future studies.

In conclusion, the present study provides the pathophysiological and mechanistic basis by which inhibition of GPR39 enhances EC-mediated angiogenesis via SHH pathway activation, resulting in the acceleration of blood perfusion recovery in ischemic tissue. Our observations could potentially open up avenues for future translational research to promote efforts designed to identify cell-specific antagonists of GPR39 for potential clinical intervention in the treatment of tissue ischemia and diabetes-related vascular complications. Indeed, the development of such small-molecule compounds would help in the further validation of our hypothesis via pharmacological approaches.

Materials and Methods

Animals. GPR39 knockout mice ($GPR39^{KO}$ on the C57BL/6 background) and their wild-type littermates ($GPR39^{WT}$) were transferred from Dr. Michal Hershfinkel's laboratory in Israel. To create an animal model of chronic hyperglycemia, we injected the animals (at the age of 16 wk) with STZ at 50 mg/kg for five consecutive days (STZ group). Citrate buffer was injected into the control (WT) group. To create a T2D model, the animals were maintained on a high-fat diet (Research Diets, D12492) from 6 wk of age for 10 wk (when at the age of 16 wk) and then received additional low-dose STZ via intraperitoneal injections for 7 d (day 1 at 50 mg/kg and days 2 to 7 at 25 mg/kg). All animal experiments were performed according to the Wayne State University Institutional Animal Care and Use Committee (IACUC) guidelines.

Cell Culture. Human aortic ECs from healthy and T2D donors were purchased from Lonza and were cultured in endothelial growth media-2 (EGM-2; Lonza, CC-3162) at 37 °C and 5% CO_2. Mouse ECs were isolated from male mice at the age of 6 to 10 wk and expanded in vitro in DMEM supplied with EC growth supplement (ECGS; 75 mg/L, Sigma) and 10% fetal bovine serum (FBS) using the previously published protocol (56). The human and mouse ECs were used between passages 5 and 7. GPR39 levels were modulated in these cells using either small interfering RNA transfection or adenovirus transfection.

Human aortic endothelial cell (HAEC) and mouse aortic endothelial cell (MAEC) Functional Assay (BrdU Proliferation, Migration, and 3D Tube Formation Assays). EC proliferation was evaluated using the BrdU Cell Proliferation Assay Kit (Cell Signaling, #6813). Optical density at 450 nm was recorded using a BioTek Epoch spectrophotometer. Cell migration was evaluated with the Boyden chamber migration assay (Transwell Costar, 6.5 mm diameter and 8 μm pore size) according to the manufacturer's instructions. Migrated cells were counted using an EVOS fluorescence microscope under ×20 magnification at four high-power random fields (HPFs). The angiogenic ability of the ECs was measured using a 3D tube formation assay. Images of the tubes were taken at three random fields per well under ×200 magnification using an EVOS fluorescence microscope.

Transcriptional Activities of GLI by GLI-luciferase Reporter Assay. The activation of the SHH pathway was measured by detecting the expression of a luciferase reporter gene under the control of a GLI-responsive promoter (GLI-luciferase). The SHH signaling was measured by detecting the luminescence before (basal) and 90 min after adding the SHH ligand at 0.1 ng/mL using a GloMax® Luminometer (Promega).

Western Blot Analysis. Procedures were performed as previously described (57). *SI Appendix*, Table S3 describes the antibodies used.

Coimmunoprecipitation Assay. Healthy ECs were transfected with the adenovirus carrying human GPR39 with a GFP tag (Ad-GFP-GPR39) or the adenovirus with only a GFP tag (Ad-GFP) as control. The Co-IP was performed according to the manufacturer's protocol using the GFP-Trap® Agarose Kit (#gtak-20, ChromoTek) to immunoprecipitate the GFP-tagged GPR39 from cell lysates. The eluted samples were analyzed by western blot. *SI Appendix*, Table S3 describes the antibodies used.

Real-Time PCR Analysis. Total RNA was extracted using the RNeasy Mini Kit (Qiagen) following the manufacturer's instructions. The primer information is shown in *SI Appendix*, Table S1.

Human Proangiogenic Protein Array. ECs at 80% confluence were transfected with Ad-GPR39 or Ad-GFP as control, and the Proteome Profiler Human Angiogenesis Array (R&D Systems, #ARY007) was performed as described previously (58).

Hind Limb Ischemia Surgery. The femoral artery was isolated from the nerves and vein. The proximal portion of the femoral artery and the distal portion of the

using DIO as obese controls. n = 5 per group, $*P < 0.05$ vs. $GPR39^{WT}$-DIO + STZ at the same time point. Representative images of blood perfusion are shown at (*I*). The collateral arteries in the media thigh muscles harvested on day 7 and day 28 after surgery were evaluated by fluorescent staining of anti-α-SMA and CD31. Representative images are shown in (*J*), and the quantification of arterial density and arterial diameter in day 28 samples are shown in (*K*) and (*L*), respectively. n = 5 per group, $**P < 0.01$. (Scale bar, 200 μm.) (*M*) The capillary density of ischemic muscle sections from $GPR39^{WT}$-DIO, $GPR39^{KO}$-DIO$GPR39^{WT}$-DIO+ STZ, and $GPR39^{KO}$-DIO+ STZ mice by CD31 fluorescent staining. n = 5 per group. $**P < 0.01$; $***P < 0.001$. Representative images are shown in the *Right* panel. (Scale bar, 400 μm.) (*N*) Incidence of tissue necrosis in $GPR39^{WT}$-DIO, $GPR39^{KO}$-DIO$GPR39^{WT}$-DIO+ STZ, and $GPR39^{KO}$-DIO+ STZ mice. n = 5 per group, $**P < 0.01$. (*O*) Body weight levels of female $GPR39^{WT}$-DIO-STZ and $GPR39^{KO}$-DIO-STZ mice receiving procedures of DIO and STZ-induced hyperglycemia over time. n = 3 per group. (*P*) Blood glucose levels of female $GPR39^{WT}$-DIO-STZ and $GPR39^{KO}$-DIO-STZ mice receiving procedures of DIO and STZ over time. n = 6 per group. (*Q*) Blood perfusion recovery in female $GPR39^{WT}$-DIO-STZ and $GPR39^{KO}$-DIO-STZ mice after hind limb ischemia. n = 6 per group. Representative images are shown in the *Right* panel. Ctrl, control limb; HLI, hind limb with ischemia. (*R*) Incidence of tissue necrosis in female $GPR39^{WT}$-DIO-STZ and $GPR39^{KO}$-DIO-STZ mice that recovered from hind limb ischemia. n = 6 per group$*P < 0.05$. Representative images are shown in the *Right* panel. In all the figures, data are represented as mean ± SD. The *P* values were first determined by the Kruskal–Wallis test across all the groups. If significant, the pairs of primary interest, based on scientific rationale, were assessed using the Mann–Whitney *U* test with Benjamini, Krieger, and Yekutieli's adjustment for multiple comparisons. The significant differences that came from post hoc comparisons of groups were noted.

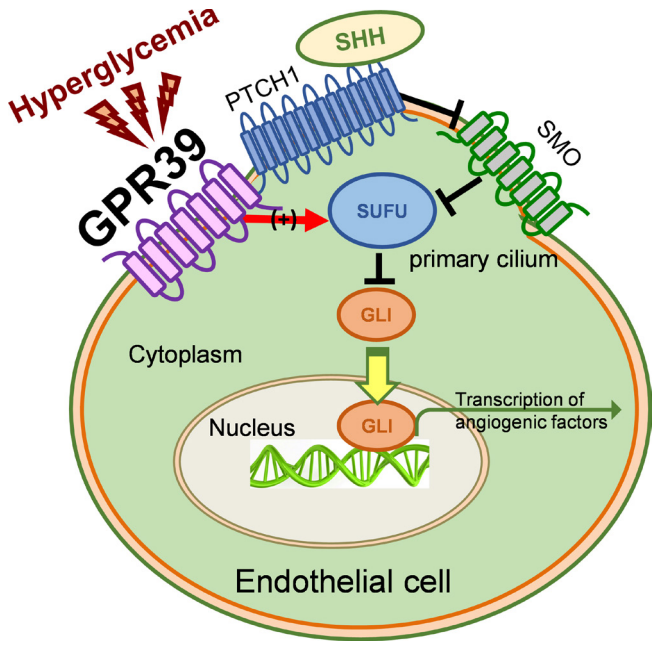

Fig. 5. Schematic hypothesis. Schematic representation of our working model based on the data accrued in our studies validating our hypothesis.

saphenous vein were ligated while the animal was under anesthesia (58). Blood flow was measured before, immediately after, and at 1, 7, 11, 14, 21, and 28 d after femoral arterial ligation using laser Doppler imaging and a PeriScan PIM 3 System (Perimed). Tissue necrosis was assessed and scored daily. *SI Appendix*, Table S2 delineates the severity of ischemia injury.

Immunofluorescent Staining. Muscle samples from hind limb ischemia studies were collected and embedded in OCT. Immunofluorescent staining was performed as previously described (58). Fluorescence images were recorded by fluorescence microscopy (EVOS; Thermo Fisher Scientific).

Statistical Analysis. All values are expressed as mean ± SD. The statistical significance of differences between the two groups was determined using the Mann–Whitney *U* test for continuous variables that failed Shapiro–Wilk normality tests, such as mRNA expression, protein levels, staining quantifications, and functional assays. In blood perfusion curve data, the two groups were tested using multiple Mann–Whitney *U* tests with Benjamini, Krieger, and Yekutieli's adjustment (59). When more than two groups of treatments were performed, the Kruskal–Wallis test was applied across all the groups, and if significant, the pairs of primary interest, based on scientific rationale, were assessed using the Mann–Whitney *U* test with Benjamini, Krieger, and Yekutieli's adjustment for multiple comparisons (59). These gatekeeping approaches and the adjustments preserved alpha spending and controlled false-positive rate inflation due to multiple hypothesis testing. The significant differences that came from post hoc comparisons of groups were noted. Similarly, for continuous variables that follow the normal distributions, such as BP and heart rates, the statistical significance of differences between the two groups was determined by Student's *t* test. When more than two treatment groups were performed, one-way ANOVA was used across all the groups. If significant, pairs of focused groups were tested with two-sample *t* tests, and *P* values were adjusted with the Benjamini, Krieger, and Yekutieli method (59). A value of $P < 0.05$ was considered statistically significant. The statistical analyses were performed using GraphPad Prism 9 (GraphPad Software).

Data, Materials, and Software Availability. All the data supporting this study's findings are included in the article and/or *SI Appendix*. The data have not been deposited in any database. An expanded *Materials and Methods* section is available in *SI Appendix*.

ACKNOWLEDGMENTS. We thank Dr. Diederik Moechars of Janssen Pharmaceuticals for providing the GPR39KO mouse colony and Dr. Michal Hershfinkel's laboratory at the Ben-Gurion University of Negev, Israel, for transferring the breeding pairs. We thank Dr. Shukkur M. Farooq at the Eugene Applebaum College of Pharmacy and Health Sciences for providing technical assistance in maintaining this strain. We also thank Dr. Wanqing Liu in the Department of Pharmaceutical Sciences and Pharmacology at the Wayne State University for his expertise in energy metabolism. We appreciate the excellent animal care provided by the Department of Laboratory Animal Research staff at the Wayne State University. This work was supported in part by NIH/NIDDK R01 DK109036, R01 DK119222, and R01 DK128937 (to J.-M.W.). A.K. was supported by R01 EY022230, Senior Research Career Scientist (K6 BX005383), and a Merit Award (BX004663) from the US Department of Veterans Affairs. M.M. was supported by the institutional training grant "IMSD at the Wayne State University" (T32 GM 139807).

Author affiliations: [a]Department of Pharmaceutical Sciences, Eugene Applebaum College of Pharmacy and Health Sciences, Wayne State University, Detroit, MI 48201; [b]Center of Molecular and Translational Medicine and the Institute of Biomedical Sciences, Georgia State University, Atlanta, GA 30303; [c]John D. Dingell Department of Veterans Affairs Medical Center, Detroit, MI 48201; [d]Institute of Molecular, Cell and Systems Biology, College of Medical, Veterinary and Life Sciences, University of Glasgow, Glasgow G12 8QQ, United Kingdom; and [e]Centers for Molecular Medicine and Genetics, Karmanos Cancer Institute, Wayne State University, Detroit, MI 48201

1. A. Farber, R. T. Eberhardt, The Current State of Critical Limb Ischemia: A Systematic Review. *JAMA surgery* **151**, 1070–1077 (2016).
2. L. Uccioli *et al.*, Critical limb ischemia: current challenges and future prospects. *Vascular health and risk management* **14**, 63–74 (2018).
3. American Diabetes Association, Peripheral arterial disease in people with diabetes. *Diabetes Care* **26**, 3333–3341 (2003).
4. D. C. Felmeden, A. D. Blann, G. Y. Lip, Angiogenesis: Basic pathophysiology and implications for disease. *Eur. Heart J.* **24**, 586–603 (2003).
5. A. A. Salybekov, A. K. Salybekova, R. Pola, T. Asahara, Sonic hedgehog signaling pathway in endothelial progenitor cell biology for vascular medicine. *Int. J. Mol. Sci.* **19**, 3040 (2018).
6. A. Avogaro, M. Albiero, L. Menegazzo, S. de Kreutzenberg, G. P. Fadini, Endothelial dysfunction in diabetes: The role of reparatory mechanisms. *Diabetes Care* **34**, S285–S290 (2011).
7. G. Sebastiani, E. Ceccarelli, M. G. Castagna, F. Dotta, G-protein-coupled receptors (GPCRs) in the treatment of diabetes: Current view and future perspectives. *Best Pract. Res. Clin. Endocrinol. Metab.* **32**, 201–213 (2018).
8. K. Sriram, P. A. Insel, G protein-coupled receptors as targets for approved drugs: How many targets and how many drugs? *Mol. Pharmacol.* **93**, 251–258 (2018).
9. K. K. McKee *et al.*, Cloning and characterization of two human G protein-coupled receptor genes (GPR38 and GPR39) related to the growth hormone secretagogue and neurotensin receptors. *Genomics* **46**, 426–434 (1997).
10. B. Holst *et al.*, GPR39 signaling is stimulated by zinc ions but not by obestatin. *Endocrinology* **148**, 13–20 (2007).
11. X. P. Huang *et al.*, Allosteric ligands for the pharmacologically dark receptors GPR68 and GPR65. *Nature* **527**, 477–483 (2015).
12. M. Hershfinkel, A. Moran, N. Grossman, I. Sekler, A zinc-sensing receptor triggers the release of intracellular Ca2+ and regulates ion transport. *Proc. Natl. Acad. Sci. U.S.A.* **98**, 11749–11754 (2001).
13. F. Bassilana *et al.*, Target identification for a Hedgehog pathway inhibitor reveals the receptor GPR39. *Nat. Chem. Biol.* **10**, 343–349 (2014).
14. J. Wang, R. Xiao, G protein-coupled receptors in energy homeostasis. *Sci. China Life Sci.* **57**, 672–680 (2014).
15. R. Romero-Nava *et al.*, Evidence of alterations in the expression of orphan receptors GPR26 and GPR39 due to the etiology of the metabolic syndrome. *J. Recept. Signal Transduct. Res.* **37**, 422–429 (2017).
16. Y. Xu, A. P. Barnes, N. J. Alkayed, Role of GPR39 in neurovascular homeostasis and disease. *Int. J. Mol. Sci.* **22**, 8200 (2021).
17. P. S. Petersen *et al.*, Deficiency of the GPR39 receptor is associated with obesity and altered adipocyte metabolism. *FASEB J.* **25**, 3803–3814 (2011).
18. B. Holst *et al.*, G protein-coupled receptor 39 deficiency is associated with pancreatic islet dysfunction. *Endocrinology* **150**, 2577–2585 (2009).
19. H. Kaur *et al.*, Single-cell profiling reveals heterogeneity and functional patterning of GPCR expression in the vascular system. *Nat. Commun.* **8**, 15700 (2017).
20. L. A. Henze *et al.*, Zinc ameliorates the osteogenic effects of high glucose in vascular smooth muscle cells. *Cells* **10**, 3083 (2021).
21. D. Zhu *et al.*, Zinc regulates vascular endothelial cell activity through zinc-sensing receptor ZnR/GPR39. *Am. J. Physiol. Cell Physiol.* **314**, C404–C414 (2018).
22. L. Chen *et al.*, G protein-coupled receptor 39 activation alleviates oxidized low-density lipoprotein-induced macrophage inflammatory response, lipid accumulation and apoptosis by inducing A20 expression. *Bioengineered* **12**, 4070–4080 (2021).
23. Q. Xiao *et al.*, Impaired sonic hedgehog pathway contributes to cardiac dysfunction in type 1 diabetic mice with myocardial infarction. *Cardiovasc Res.* **95**, 507–516 (2012).
24. C. Di Mauro *et al.*, Hedgehog signalling pathway orchestrates angiogenesis in triple-negative breast cancers. *Br. J. Cancer* **116**, 1425–1435 (2017).

25. R. Pola *et al.*, Postnatal recapitulation of embryonic hedgehog pathway in response to skeletal muscle ischemia. *Circulation* **108**, 479–485 (2003).
26. H. Fernandes-Silva, J. Correia-Pinto, R. S. Moura, Canonical sonic hedgehog signaling in early lung development. *J. Dev. Biol.* **5**, 3 (2017).
27. I. Deshpande *et al.*, Smoothened stimulation by membrane sterols drives Hedgehog pathway activity. *Nature* **571**, 284–288 (2019).
28. D. Lainez-Gonzalez, J. Serrano-Lopez, J. M. Alonso-Dominguez, Understanding the hedgehog signaling pathway in acute myeloid leukemia stem cells: A necessary step toward a cure. *Biology* **10**, 255 (2021).
29. G. B. Carballo, J. R. Honorato, G. P. F. de Lopes, T. Spohr, A highlight on Sonic hedgehog pathway. *Cell Commun. Signal.* **16**, 11 (2018).
30. J. M. Wang, J. S. Isenberg, T. R. Billiar, A. F. Chen, Thrombospondin-1/CD36 pathway contributes to bone marrow-derived angiogenic cell dysfunction in type 1 diabetes via Sonic hedgehog pathway suppression. *Am. J. Physiol. Endocrinol. Metab.* **305**, E1464–E1472 (2013).
31. R. Gupta *et al.*, Endothelial smoothened-dependent hedgehog signaling is not required for sonic hedgehog induced angiogenesis or ischemic tissue repair. *Lab. Invest.* **98**, 682–691 (2018).
32. S. Dittmer *et al.*, The constitutively active orphan G-protein-coupled receptor GPR39 protects from cell death by increasing secretion of pigment epithelium-derived growth factor. *J Biol Chem.* **283**, 7074–7081 (2008).
33. B. Holst *et al.*, Common structural basis for constitutive activity of the ghrelin receptor family. *J Biol Chem.* **279**, 53806–53817 (2004).
34. Y. Xu, S. Song, Z. Wang, J. A. Ajani, The role of hedgehog signaling in gastric cancer: Molecular mechanisms, clinical potential, and perspective. *Cell Commun. Signal* **17**, 157 (2019).
35. M. Simons *et al.*, State-of-the-art methods for evaluation of angiogenesis and tissue vascularization: A scientific statement from the American heart association. *Circ. Res.* **116**, e99–e132 (2015).
36. Z. Aref, M. R. de Vries, P. H. A. Quax, Variations in surgical procedures for inducing hind limb ischemia in mice and the impact of these variations on neovascularization assessment. *Int. J. Mol. Sci.* **20**, 3704 (2019).
37. V. van Weel *et al.*, Hypercholesterolemia reduces collateral artery growth more dominantly than hyperglycemia or insulin resistance in mice. *Arterioscler. Thromb. Vasc. Biol.* **26**, 1383–1390 (2006).
38. J. P. Cooke, D. W. Losordo, Modulating the vascular response to limb ischemia: Angiogenic and cell therapies. *Circ. Res.* **116**, 1561–1578 (2015).
39. T. S. Westvik *et al.*, Limb ischemia after iliac ligation in aged mice stimulates angiogenesis without arteriogenesis. *J. Vasc. Surg.* **49**, 464–473 (2009).
40. P. D. O'Brien *et al.*, Juvenile murine models of prediabetes and type 2 diabetes develop neuropathy. *Dis. Model. Mech.* **11**, dmm037374 (2018).
41. A. A. Rossini, R. M. Williams, M. C. Appel, A. A. Like, Sex differences in the multiple-dose streptozotocin model of diabetes. *Endocrinology* **103**, 1518–1520 (1978).
42. A. E. Salinero, B. M. Anderson, K. L. Zuloaga, Sex differences in the metabolic effects of diet-induced obesity vary by age of onset. *Int. J. Obes.* **42**, 1088–1091 (2018).
43. E. H. Leiter, Multiple low-dose streptozotocin-induced hyperglycemia and insulitis in C57BL mice: Influence of inbred background, sex, and thymus. *Proc. Natl. Acad. Sci. U.S.A.* **79**, 630–634 (1982).
44. C. Le May *et al.*, Estrogens protect pancreatic beta-cells from apoptosis and prevent insulin-deficient diabetes mellitus in mice. *Proc. Natl. Acad. Sci. U.S.A.* **103**, 9232–9237 (2006).
45. P. S. Petersen *et al.*, Deficiency of the GPR39 receptor is associated with obesity and altered adipocyte metabolism. *FASEB J.* **25**, 3803–3814 (2011).
46. F. Tremblay *et al.*, Normal food intake and body weight in mice lacking the G protein-coupled receptor GPR39. *Endocrinology* **148**, 501–506 (2007).
47. S. W. Lee, M. A. Moskowitz, J. R. Sims, Sonic hedgehog inversely regulates the expression of angiopoietin-1 and angiopoietin-2 in fibroblasts. *Int. J. Mol. Med.* **19**, 445–451 (2007).
48. E. Mathew *et al.*, The transcription factor GLI1 modulates the inflammatory response during pancreatic tissue remodeling. *J. Biol. Chem.* **289**, 27727–27743 (2014).
49. J. Kitlinska *et al.*, Dual role of dipeptidyl peptidase IV (DPP IV) in angiogenesis and vascular remodeling. *Adv. Exp. Med. Biol.* **524**, 215–222 (2003).
50. J. Zhong, A. Maiseyeu, S. N. Davis, S. Rajagopalan, DPP4 in cardiometabolic disease: Recent insights from the laboratory and clinical trials of DPP4 inhibition. *Circ. Res.* **116**, 1491–1504 (2015).
51. T. Hara *et al.*, Physiological roles of zinc transporters: Molecular and genetic importance in zinc homeostasis. *J. Physiol. Sci.* **67**, 283–301 (2017).
52. D. Zhu *et al.*, Zinc regulates vascular endothelial cell activity through zinc-sensing receptor ZnR/GPR39. *Am. J. Physiol. Cell Physiol.* **304**, C404–C414 (2018).
53. Y. Xu *et al.*, Activation of GPR39 with the agonist TC-G 1008 ameliorates ox-LDL-induced attachment of monocytes to endothelial cells. *Eur. J. Pharmacol.* **858**, 172451 (2019).
54. D. Donnini, G. Perrella, G. Stel, F. S. Ambesi-Impiombato, F. Curcio, A new model of human aortic endothelial cells in vitro. *Biochimie* **82**, 1107–1114 (2000).
55. J. K. Hennigs, C. Matuszcak, M. Trepel, J. Korbelin, Vascular endothelial cells: Heterogeneity and targeting approaches. *Cells* **10**, 2712 (2021).
56. J. M. Wang, A. F. Chen, K. Zhang, Isolation and primary culture of mouse aortic endothelial cells. *J. Vis. Exp.* **118**, 52965 (2016).
57. H. Li *et al.*, Novel role of GPR35 (G-protein-coupled receptor 35) in the regulation of endothelial cell function and blood pressure. *Hypertension* **78**, 816–830 (2021).
58. H. Nguyen *et al.*, A novel imidazolinone metformin-methylglyoxal metabolite promotes endothelial cell angiogenesis via the eNOS/HIF-1α pathway. *Faseb j* **35**, e21645 (2021).
59. Y. Benjamini, A. M. Krieger, D. Yekutieli, Adaptive linear step-up procedures that control the false discovery rate. *Biometrika* **93**, 491–507 (2006).